Journal of Hazardous Materials 181 (2010) 708–715

Contents lists available at ScienceDirect

Journal of Hazardous Materials

journal homepage: www.elsevier.com/locate/jhazmat

Photocatalytic degradation of 1-naphthol by oxide ceramics with added bacterial disinfection

Chockalingam Karunakaran*, Sona Narayanan, Paramasivan Gomathisankar

Department of Chemistry, Annamalai University, Annamalainagar 608002, Tamilnadu, India

ARTICLE INFO

Article history:
Received 25 February 2010
Received in revised form 14 May 2010
Accepted 15 May 2010
Available online 9 June 2010

Keywords:
α-Naphthol
Semiconductor
Photodegradation
Bactericidal activity

ABSTRACT

1-Naphthol photodegrades on the surfaces of TiO_2, ZnO, CeO_2, CdO, WO_3, Co_3O_4, Sb_2O_3, ZrO_2, La_2O_3, Y_2O_3, Pr_6O_{11}, Sm_2O_3 and Al_2O_3, albeit at different efficiencies, and all the oxides show sustainable photocatalytic activity. The degradation conforms to the Langmuir-Hinshelwood kinetic model and enhances with the intensity of illumination. Dissolved oxygen is essential for the degradation. ZnO and TiO_2 anatase are the most efficient photocatalysts to degrade 1-naphthol. ZnO wurtzite, besides serving as an effective photocatalyt to degrade 1-naphthol, also acts as a bactericide; it inactivates *E.coli* even in absence of direct light. At a loading of 0.8 g L^{-1}, it kills about 44% of 2.5×10^{12} CFU mL^{-1} *E. coli* in ½ h under dark condition.

1. Introduction

1-Naphthol, a large-scale industrial chemical used for the manufacture of dyes, insecticides, etc., is a metabolite of the widely used insecticide carbaryl (1-naphthyl methylcarbamate, marketed under the brand name Sevin) and is hazardous. Also, it affects the reproductive hormone levels in adult men [1]. While a few reports are available on photocatalytic degradation of 2-naphthol [2–7] there is none on 1-naphthol; the latter is reported to be more toxic than the former in causing mitotic disturbance, the depolymerization of spindle microtubules [8]. Photocatalytic oxidation is one of the emerging techniques for the elimination of organic micro pollutants because of its efficiency of mineralization, ideally produce carbon dioxide and water as end products at ambient conditions. Shining semiconductors with light of energy not less than the band gap creates electron-hole pairs, holes in the valence band and electrons in the conduction band. Some of these pairs diffuse out to the crystal surface and react with the adsorbed substrates resulting in photocatalysis [9]. The hole reacts with the adsorbed organics generating intermediates [10], which through fast reactions finally yield carbon dioxide and water [11–14]. The adsorbed oxygen molecule takes up the conductance band electron transforming into highly active superoxide radical, $O_2^{\bullet -}$ [9]. In aqueous medium, $O_2^{\bullet -}$ in turn generates reactive species like $HO^{\bullet}$, $HO_2^{\bullet}$ and H_2O_2, which oxidize the organics. Water is adsorbed on the semiconductor, molecularly as well as dissociatively [15,16]. Hole trapping by either the surface hydroxyl groups or the adsorbed water molecules yields short-lived $HO^{\bullet}$ radicals, which are the primary oxidizing agents [17–20]. TiO_2 is a promising candidate for photocatalytic material application due to its exceptional optical and electronic properties, chemical stability, non-toxicity and low cost [21,22]. The band gap of ZnO is almost the same that of TiO_2 and the conduction and valence band edges of the former are very close to those of the latter [23], and hence the former has also been tested as catalyst for 1-naphthol photodegradation. Visible light active narrow band gap semiconductor such as CdO, and UV-C light active supra band gap oxides like ZrO_2, La_2O_3 and Sm_2O_3 have also been included as test photocatalysts for the degradation of 1-naphthol. Use of Al_2O_3, an insulator, provides a comparison.

Bacterial contamination and growth in water are potential health hazards demanding disinfection. Now, the use of inorganic antimicrobial agents, compared to the organics, has attracted interest due to their improved safety and stability [24,25]; ceramics with inherent bactericidal activity are convenient to use as they are insoluble. Our results reveal that ZnO, besides acting as an efficient catalyst to photodegrade 1-naphthol, exhibits antimicrobial activity. That is, ZnO provides a two-in-one advantage, better photocatalyzed degradation of 1-naphthol with bacterial disinfection. In this study *Escherichia coli* (*E. coli*) is used as an index to assess the bactericidal activity.

2. Experimental

2.1. Materials

1-Naphthol (E Merck) was recrystallized from ethanol before use. TiO_2 (Merck), ZnO (Merck), Co_3O_4 (Merck), Al_2O_3 (Merck), WO_3 (Sigma Aldrich), Sb_2O_3 (Qualigens), CeO_2 (Sd fine), Y_2O_3 (Sd

* Corresponding author. Tel.: +919443481590; fax: +914144238145.
E-mail address: karunakaranc@rediffmail.com (C. Karunakaran).

0304-3894/$ – see front matter © 2010 Elsevier B.V. All rights reserved.
doi:10.1016/j.jhazmat.2010.05.070

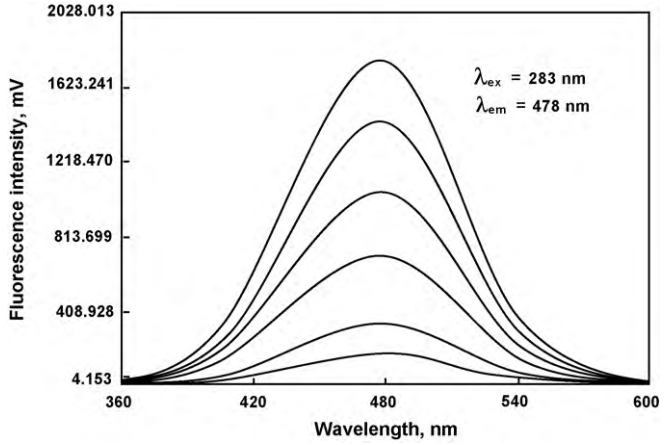

Fig. 1. Fluorescence spectra of 100-times diluted 0.01, 0.02, 0.04, 0.06, 0.08 and 0.10 mM 1-naphthol.

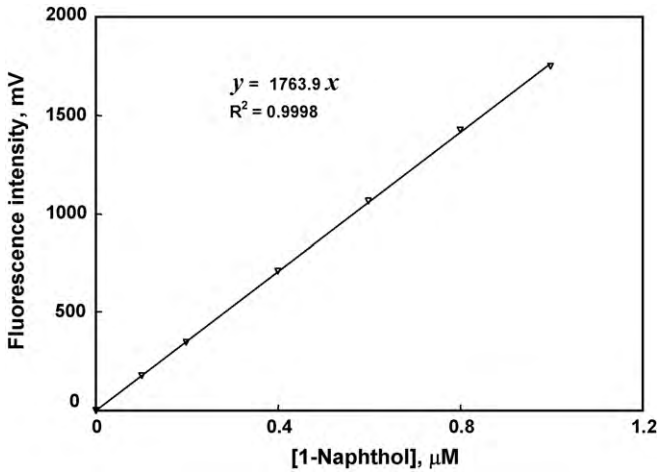

Fig. 2. Fluorescence intensity–concentration curve.

fine), Pr_6O_{11} (Sd fine), Sm_2O_3 (Sd fine), La_2O_3 (Himedia), CdO (Chemco) and ZrO_2 (Chemco) were of analytical grade and used as received. Other chemicals used were also of analytical or laboratory grade.

2.2. Characterization

The powder XRDs of the oxides were recorded using a Siemens D5000 XRD employing Cu K_α X-rays of wavelength 1.5406 Å with a tube current of 30 mA at 40 kV under a scan range of 5-60° at a scan speed of 0.2° s^{-1} or a Bruker D8 system using Cu K_α radiation of 1.5406 Å in a 2θ range of 5-60° at a scan speed of 0.050° s^{-1} or a Rich Seifert model 3000 X-ray diffractrometer. The specific surface areas of the oxides were determined by the nitrogen-adsorption desorption method using the Brunauer-Emmett-Teller (BET) equation. A PerkinElmer Lamda 35 spectrometer was employed to record the UV-visible diffuse reflectance spectra (DRS) of the oxides.

2.3. Photoreactor

Photodegradation of 1-naphthol was carried out in a multilamp photoreactor fitted with eight 8 W mercury lamps of wavelength 365 nm (Sankyo Denki, Japan) and highly polished anodized aluminum reflector; the reaction tube was placed at the centre. Four cooling fans fitted at the bottom of the reactor dissipate the generated heat. The reaction vessel was borosilicate glass tube of 15-mm inner diameter. The reactor was illuminated by using two or four or eight lamps; the angles sustained by the adjacent lamps at the sample were 180°, 90° and 45°, respectively. The light intensities were determined by ferrioxalate actinometry [26].

2.4. Estimation of 1-naphthol

Solution of 1-napthol of desired concentration in deionized distilled water was prepared and its UV-visible spectrum was recorded, using a UV-1650 Shimadzu spectrophotometer, to determine the wavelength of excitation for its spectrofluorimetic analysis. Fig. 1 presents the fluorescence spectra of 1-napthol solutions of different concentrations recorded using an Elico SL 174 spectrofluorimeter; the wavelength of excitation was set at 283 nm. Fig. 2 is the calibration curve, constructed using the measured intensity of emission at 478 nm. This calibration curve was used to estimate 1-naphthol in a solution by measuring its fluorescence intensity, after appropriate stepwise dilution.

2.5. Photodegradation

Fresh solution of 1-naphthol of required concentration (ca. 0.05 to 0.4 mM) was prepared and used for the photodegradation study. Air was bubbled through 20 mL of the solution which effectively kept the added catalyst under suspension and at continuous motion. The air-flow rate was measured by soap bubble method. A time lag of at least 15 min was provided before illumination to ensure pre-adsorption of the naphthol and oxygen on the oxide. After illumination, the oxide was recovered by centrifugation and the naphthol was estimated fluorimetrically, after stepwise dilution up to 500-times. The exponential decrease in naphthol-concentration for a finite time of illumination (3, 5, 10 or 30 min) provided the degradation rate and the results were reproducible to ±5%. Atomic absorption spectra of the naphthol solutions illuminated with the active oxide and recorded using an Elico SL 176 double beam atomic absorption spectrometer, show absence of noticeable dissolution of the oxide. The unadjusted experimental pH was between 6 and 8 (Table 1); however, with WO_3 the pH drops to about 5. The light intensity was varied by using two, four and eight lamps. The dissolved oxygen was measured using an Elico dissolved oxygen analyzer PE 135, the solution UV-visible spectral studies were made with UV-1650 Shimadzu spectrophotometer.

2.6. Bacterial culture

A nutrient broth culture medium of pH 7.4 was obtained by dissolving 13.0 g nutrient broth (5.0 g peptone, 5.0 g NaCl, 2.0 g yeast extract, 1.0 g beef extract) in 1 L distilled water followed by sterilization in an autoclave at 121 °C. MacConkey agar plates were prepared separately by dissolving 55 g MacConkey agar (20 g peptic digest of animal tissue, 10 g lactose, 5 g sodium taurocholate, 0.04 g neutral red, 20 g agar) in 1 L boiling distilled water followed by ster-

Table 1
pH of 1-naphthol solution with oxide.

Oxide	TiO_2	ZnO	CeO_2	CdO	WO_3	Co_3O_4	Sb_2O_3	ZrO_2	La_2O_3	Y_2O_3	Pr_6O_{11}	Sm_2O_3	Al_2O_3
pH[a]	7.1	7.2	7.6	8.4	4.8	8.0	6.5	6.5	7.2	6.9	7.5	7.2	7.2

[a] 20 mL 0.423 mM naphthol, 0.10 g oxide loading, 19.2 mg L^{-1} dissolved O_2.

ilization in an autoclave at 121 °C and poured into Petri dish. *E. coli* was inoculated in 10 mL of a nutrient broth and incubated for 24 h at 37 °C. The culture was centrifuged at 3500 rpm and the pellet obtained was washed with 0.9% NaCl (autoclaved) solution, twice and suspended in 50 mL of 0.9% NaCl solution. For the counting of *E. coli* colonies in CFU mL^{-1}, the bacterial solution was successively diluted to 10^9-times using 0.9% NaCl solution in order to achieve about 100 to 200 colonies on the Petri dish [27]; using a loop, 10 μL of the diluted *E. coli* was streaked on the MacConkey agar plate and incubated at 37 °C for 24 h. The CFU was counted by a viable count method [27].

2.7. Bactericidal study

20 mg of ZnO was added to 25 mL of *E. coli* solution taken in a 150 mL bottle and shaken well continuously without any illumination. After a finite time (30 min), a finite volume (1 mL) of *E. coli* solution was removed from the oxide, diluted stepwise and enumerated as already stated.

3. Results and discussion

3.1. Catalysts characterization

The TiO_2 used is of anatase phase; its XRD pattern totally matches with the standard pattern of anatase (JCPDS 00-021-1272*) and the rutile lines (00-034-0180 D) are absent. The crystal is tetragonal body-centered and the crystal parameters *a* and *c* are 3.7845 and 9.5143 Å, respectively. The XRD of ZnO is identical with the JCPDS pattern of zincite (00-005-0664 D) and reveals the crystal structure as hexagonal primitive with the cell constants *a* and *b* as 3.2490 Å and *c* as 5.2050 Å. The XRD of WO_3 agrees with its JCPDS pattern (89-4476) revealing monoclinic primitive crystal structure with crystal parameters *a*, *b* and *c* as 7.3291 Å, 7.5006 Å and 7.6718 Å, and α, β and γ as 90.0°, 88.18 ± 2.89° and 90.0°, respectively. The XRD of CeO_2 totally matches with the standard JCPDS pattern of CeO_2 (898436) and reveals the crystal structure as face centered cubic system with *a* as 5.411 Å. The XRD of Al_2O_3 matches with the standard JCPDS patterns of γ-Al_2O_3 (00-001-1308 D, cubic *a* 7.900 Å) and χ -Al_2O_3 (00-004-0880 N, cubic *a* 7.950 Å) revealing the presence of both the phases (γ:χ::52:48). The BET surface areas (*S*), determined by the N_2-adsorption-desorption method, are: TiO_2 14.68, ZnO 12.16, CdO 14.45, CeO_2 11.0, WO_3 39.1, ZrO_2 15.12, Y_2O_3 10.97, Al_2O_3 10.63 $m^2\ g^{-1}$. The mean particle sizes (*D*) of the oxides, obtained by using the relationship, $D = 6/\rho S$ [28], where ρ is the material density, are as follows: TiO_2 104, ZnO 87, CdO 51, CeO_2 57, WO_3 23, ZrO_2 68, Y_2O_3 109, Al_2O_3 167 nm. Fig. 3, the diffuse reflectance spectra (DRS) of the oxides in terms of Kubelka-Munk function (K/S), shows that ZnO, TiO_2, CeO_2, WO_3 and Sb_2O_3 undergo band gap excitation at the wavelength of illumination; the visible light absorption of the CdO used is very weak. Al_2O_3 is an insulator and ZrO_2, Y_2O_3, La_2O_3 and Sm_2O_3 are wide band gap oxides; the DRS confirm that these oxides are not excited by the UV-A illumination. Pr_6O_{11} and Co_3O_4 are black.

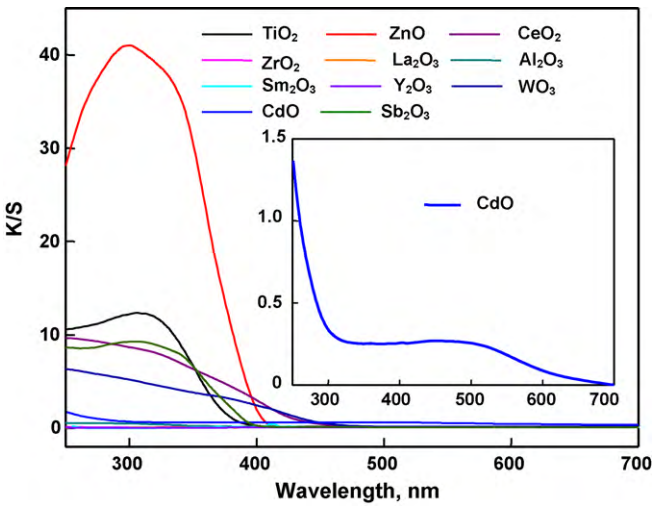

Fig. 3. The diffuse reflectance spectra.

3.2. Characteristics of photocatalytic degradation

3.2.1. Langmuir-Hinshelwood kinetics

1-Naphthol degrades on TiO_2, ZnO, CeO_2, CdO, WO_3, Co_3O_4, Sb_2O_3, ZrO_2, La_2O_3, Y_2O_3, Pr_6O_{11}, Sm_2O_3 and Al_2O_3 crystal surfaces under UV-A light, albeit at different ease. The spectrofluorimetric studies show continuous removal of 1-naphthol on the listed oxides under UV-A illumination. Fig. 4 displays the spectrofluorimetric time-scans of 1-naphthol solution illuminated at 365 nm with ZnO or Pr_6O_{11}. The degradation by ZnO and TiO_2 are fast. Fig. 5 displays the decay of 1-naphthol with illumination time on all the oxides studied. The variations of degradation rates with 1-naphthol-concentration are presented in Fig. 6. While the degradation on WO_3, La_2O_3, Pr_6O_{11} and Sm_2O_3 surfaces enhances linearly with 1-naphthol-concentration that on other oxides conforms to the Langmuir-Hinshelwood kinetic law given below.

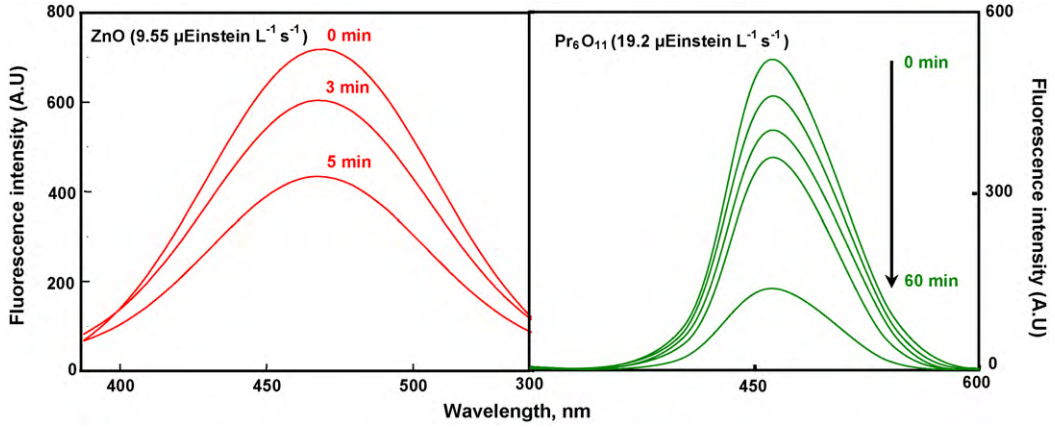

Fig. 4. Fluorescence spectral time scan of naphthol illuminated with oxide (under 50-times dilution). 20 mL 0.423 mM 1-naphthol, 0.10 g oxide loading, 7.8 mL s^{-1} airflow, 19.2 mg L^{-1} dissolved O_2, 365 nm.

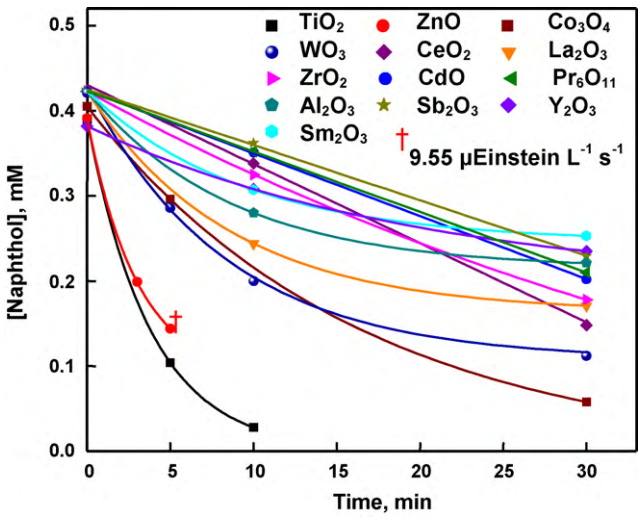

Fig. 5. Decay of 1-naphthol with illumination time. 0.10 g oxide loading, 7.8 mL s^{-1} airflow, 19.2 mg L^{-1} dissolved O_2, 365 nm, 19.2 μEinstein L^{-1} s^{-1}, 20 mL naphthol solution.

$$\textit{Degradation rate} = kK[\text{1-}\textit{Naphthol}]/(1 + K[\text{1-}\textit{Naphthol}]),$$

where K is the adsorption coefficient of 1-naphthol on the illuminated surface of the oxide and k is the surface pseudo-first-order rate constant. If the adsorption coefficient on the illuminated surface is too small so that $1 \gg K[\text{1-Naphthol}]$, the Langmuir-Hinshelwood kinetic equation reduces to the following simple first-order kinetic law.

$$\textit{Degradation rate} = k^*[\text{1-}\textit{Naphthol}]$$

where k^* is the first-order rate constant and is equal to kK. That is, the degradation follows first-order kinetics under the experimental conditions studied. This accounts for the observed different photokinetic behaviors on the oxides. Table 2 presents the first-order rate constants of the photodegradation on WO_3, La_2O_3, Pr_6O_{11} and Sm_2O_3 surfaces. The adsorption coefficient employed in the Langmuir-Hinshelwood kinetic model corresponds to photoadsorption, the adsorption on illuminated surface, which is different from the experimentally determinable dark adsorption coefficient. The photoadsorption coefficient (K) could be deduced by fitting the photodegradation data to the kinetic law. Table 3 presents the deduced Langmuir-Hinshelwood kinetic constants. They have been obtained by fitting the experimental data to a curve governed by the Langmuir-Hinshelwood kinetic equation and drawn using a C++ program [29]. Fig. 7 is the graphical display of the data fit using the kinetic constants listed in Table 3; the experimental results are plotted against the predicted ones based on the Langmuir-Hinshelwood kinetic law. The results of adsorption experiments in absence of direct light, presented in Table 4, show that photoadsorption is different from dark adsorption. While the dark adsorption of 1-naphthol on CdO, Sb_2O_3, CeO_2, Al_2O_3, etc., are insignificant the photoadsorption are not so; the degradation on these oxides follows Langmuir-Hinshelwood kinetics. Conversely, although the dark adsorption on WO_3 is large, the photoadsorption is insignificant and the photodegradation conforms to the first-order rate law. However, the photoadsorption on La_2O_3, Pr_6O_{11} and Sm_2O_3 surfaces reflects the dark adsorption; these surfaces display first-order photokinetics.

Table 2
The first-order rate constants (k^*)[a].

	WO_3	La_2O_3	Pr_6O_{11}	Sm_2O_3
10^3k^* (s^{-1})	1.04	0.52	0.19	0.54

[a] 0.10 g oxide loading, 20 mL naphthol solution, 7.8 mL s^{-1} airflow rate, 19.2 mg L^{-1} dissolved O_2, 365 nm, 19.2 μEinstein L^{-1} s^{-1}.

3.2.2. Other characteristics

The oxides show sustainable photocatalytic activity and do not loose their efficiencies on illumination. Recycling of the oxides without any pre-treatment provides almost identical results; Table 5 presents the photocatalytic efficiencies of fresh and recycled oxides. After illumination with naphthol, the oxides were collected at centrifuge, washed with water thoroughly and dried for reuse.

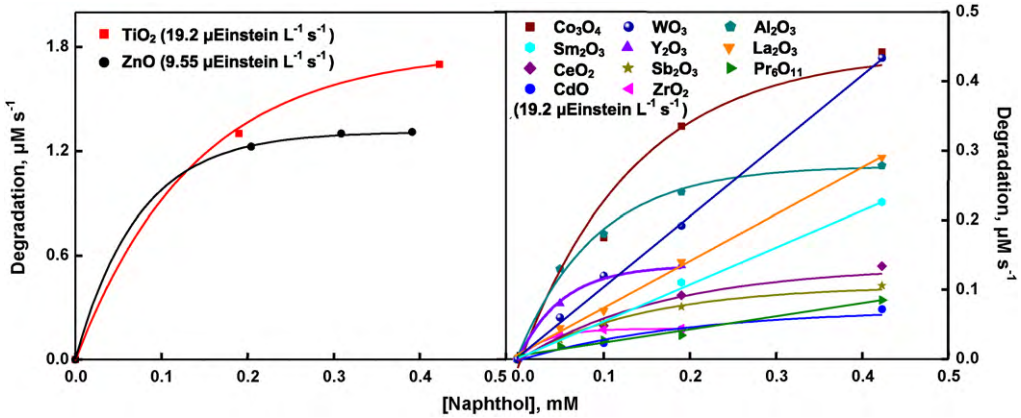

Fig. 6. Dependence of degradation rates on naphthol-concentration. 0.10 g oxide loading, 7.8 mL s^{-1} airflow, 19.2 mg L^{-1} dissolved O_2, 365 nm,19.2 μEinstein L^{-1} s^{-1}, 20 mL 1-naphthol solution.

Table 3
The Langmuir-Hinshelwood kinetic parameters.[a].

	ZnO[b]	TiO_2	CeO_2	CdO	Co_3O_4	Sb_2O_3	ZrO_2	Y_2O_3	Al_2O_3
K (mM^{-1})	29.4	5.1	2.5	1.3	2.0	3.2	14.7	16.6	13.2
k (μM s^{-1})	1.43	2.6	0.28	0.20	1.00	0.20	0.06	0.18	0.33

[a] 0.10 g oxide loading, 20 mL naphthol solution, 7.8 mL s^{-1} airflow rate, 19.2 mg L^{-1} dissolved O_2, 365 nm, 19.2 μEinstein L^{-1} s^{-1}.
[b] 9.54 μEinstein L^{-1} s^{-1}.

Table 4
Adsorption of 1-naphthol in dark.

	TiO_2	ZnO	CeO_2	CdO	WO_3	Co_3O_4	Sb_2O_3	ZrO_2	La_2O_3	Y_2O_3	Pr_6O_{11}	Sm_2O_3	Al_2O_3
Adsorption[a] (%)	16	5	1	0	24	26	1	29	7	29	9	2	0

[a] 20 mL 0.423 mM naphthol, 0.10 g oxide loading, 7.8 mL s^{-1} airflow, 19.2 mg L^{-1} dissolved O_2.

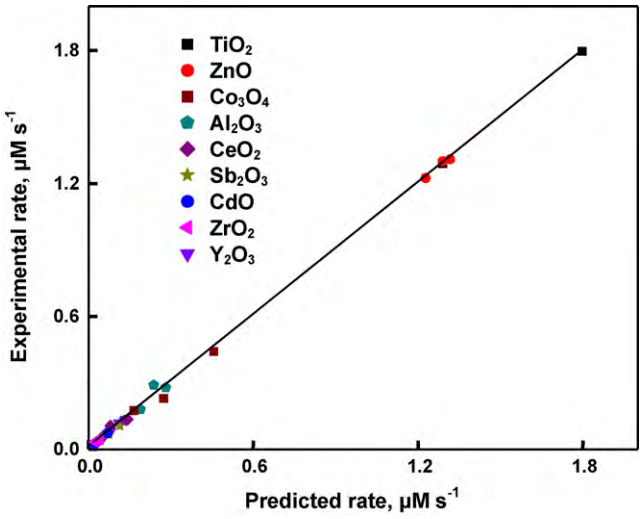

Fig. 7. Graphical display of Langmuir-Hinshelwood kinetic data fit.

The photodegradation requires dissolved oxygen. Deaeration of naphthol solution by purging nitrogen instead of air practically arrests the degradation in all the cases and Table 6 presents the measured degradation rates at different concentrations of dissolved oxygen. Fig. 8 shows the dependence of the degradation on the intensity of illumination; the enhancement of degradation with the photon flux is nonlinear. Generally, the photocatalytic rate is to vary linearly with the light intensity at low photon flux but at high light intensity its dependence is on the square-root of photon flux [29,30]. The present results conform to the same. However, ZrO_2 and Y_2O_3 are the exceptions; the degradation on these two oxides depends linearly on the photon flux. The degradation on ZnO and TiO_2 is fast at high photon flux and could not be measured. In all the cases, the loss of naphthol due to photolysis is small.

3.3. Photocatalytic mechanism

The mechanism of degradation of organics on band gap-illuminated semiconductor surfaces is well known and has been stated already. Fig. 3, the diffuse reflectance spectra, reveals that ZrO_2, La_2O_3, Y_2O_3, Sm_2O_3 and Al_2O_3 do not significantly absorb UV-A light. It is known that the emission spectrum of the medium

Table 5
Sustainable photocatalysis.

Oxide	Degradation[a] (%)												
	TiO_2	ZnO	CeO_2	CdO	WO_3	Co_3O_4	Sb_2O_3	ZrO_2	La_2O_3	Y_2O_3	Pr_6O_{11}	Sm_2O_3	Al_2O_3
Fresh	92	100	17	10	69	84	14	8	42	19	12	27	34
Recycled	92	100	17	10	69	84	14	8	42	19	12	27	34

[a] 20 mL 0.423 mM naphthol, 0.10 g oxide loading, 7.8 mL s^{-1} airflow, 19.2 mg L^{-1} dissolved O_2, 365 nm, 19.2 μEinstein L^{-1} s^{-1}, 10 min.

Table 6
Dissolved O_2 and degradation.

$[O_2]_{dissolved}$ (mg L^{-1})	Degradation[a] (%)												
	TiO_2	ZnO	CeO_2	CdO	WO_3	Co_3O_4	Sb_2O_3	ZrO_2	La_2O_3	Y_2O_3	Pr_6O_{11}	Sm_2O_3	Al_2O_3
19.2	92	100	17	10	69	84	14	8	42	19	12	27	34
2.4	0	0	0	0	0	0	0	0	0	0	1	1	1

[a] 20 mL 0.423 mM naphthol, 0.10 g oxide loading, 365 nm, 19.2 μEinstein L^{-1} s^{-1}, 10 min.

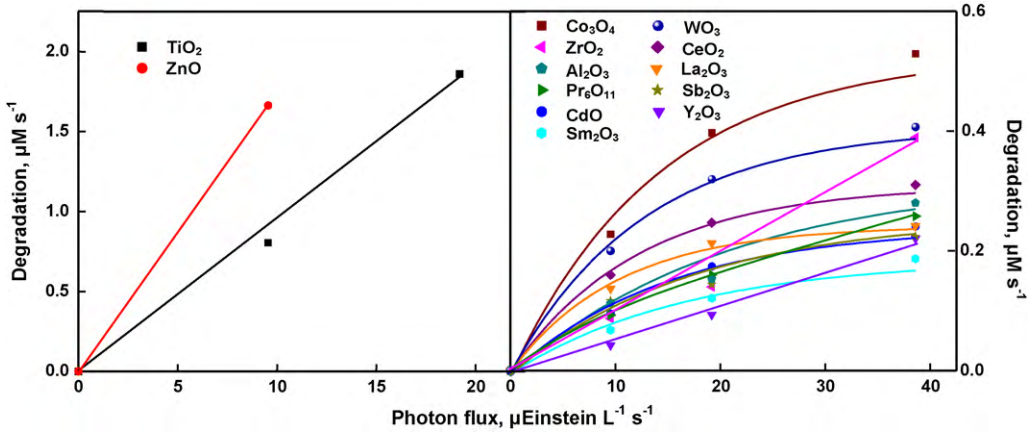

Fig. 8. Dependence of degradation rates on photon flux. 20 mL 0.423 mM 1-naphthol, 0.10 g oxide loading, 7.8 mL s^{-1} airflow, 19.2 mg L^{-1} dissolved O_2, 365 nm.

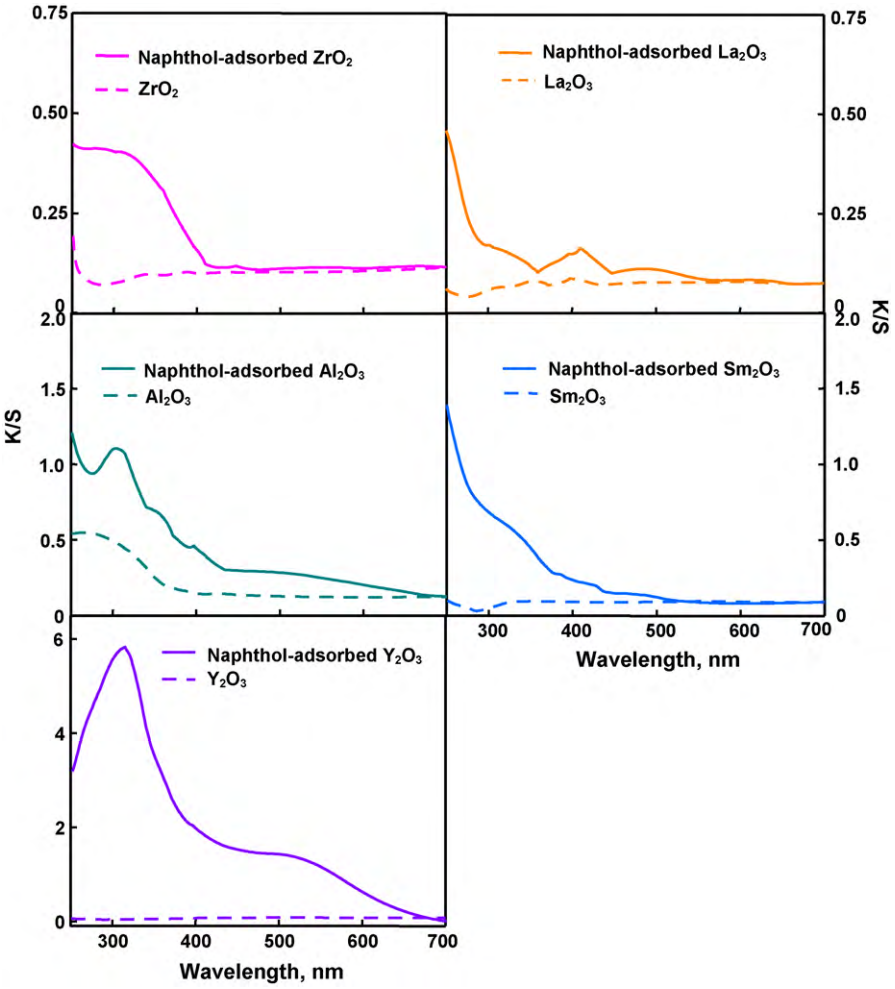

Fig. 9. The diffuse reflectance spectra of 1-naphthol-adsorbed ZrO_2, La_2O_3, Y_2O_3, Sm_2O_3 and Al_2O_3.

pressure Hg-lamp, in addition to the strong 365 nm line (I-line), shows a number of less intense other lines at 254, 405 (H-line) and 436 nm (G-line). The used borosilicate reaction vessel screens the UV-C light (254 nm line). Hence, the possibility of direct activation of these oxides by the employed medium pressure Hg-lamp is excluded. Analytical experiments reveal adsorption of the naphthol on these oxides (Table 4). The acidic cationic sites on the surface of oxides may coordinate with the naphtholic oxygen and/or the basic O^-group may be involved in hydrogen bonding with the -OH group of naphthol. The possible mechanism is light absorption by 1-naphthol-adsorbed oxides; an electron from the nonbonding orbital may be excited. Fig. 9, the diffuse reflectance spectra of 1-naphthol-adsorbed ZrO_2, La_2O_3, Y_2O_3, Sm_2O_3 and Al_2O_3, confirms the same; the spectra of bare oxides are displayed for comparison. While the naphthol-adsorbed oxides absorb light at the wavelength of illumination the bare oxides fail to do so. A possible reason for the observed high photocatalytic activity of ZnO is its high absorptivity (Kubelka-Munk function, K/S) at the wavelength of illumination, as shown by Fig. 3. Large photoadsorption of 1-naphthol on ZnO surface (Table 3) may also lead to high photodegradation rate.

3.4. Antibacterial activity

Fig. 10 reveals the *E. coli* inactivation by suspended ZnO in absence of direct light. The bactericidal efficiency of ZnO in a population of 2.5×10^{12} CFU mL^{-1} is 44% in ½ h. In absence of ZnO the *E. coli* population remains unchanged during the experimental period displaying the antibacterial activity of ZnO. But, experiment with TiO_2 under identical conditions fails to show any significant inactivation of the bacteria. *E. coli* in 0.9% saline was used for the evaluation of the antibacterial activity. The cell population was determined by a viable count method on MacConkey agar plates after proper dilution of the culture. The antibacterial efficiency is

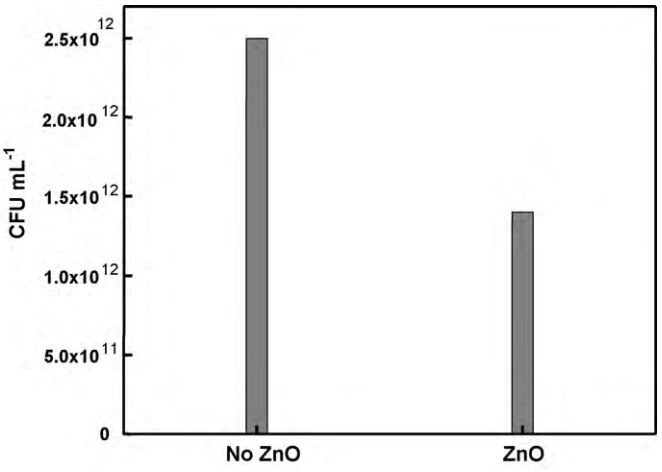

Fig. 10. *E. Coli* inactivation by ZnO without direct light in 30 min. 0.8 g L^{-1} oxide loading, pH 7.4.

the ratio of the decrease of *E. coil* population at a given time to its initial population; antibacterial efficiency = 100 $(C_0–C_t)/C_0$, where C_t and C_0 are the *E. coli* population at time t and zero, respectively.

3.5. Antibacterial mechanism

Although there are a few reports on the inactivation of *E. coli* by metal oxide nanoparticles and bulk particles in absence of any illumination, the mechanism of action still remains obscure [24,25,27,31]. In spite of the detected release of Zn^{2+} from ZnO suspension [24,31] examination of *E. coli* inactivation by added Zn^{2+} ions separately shows that the Zn^{2+} ion release from ZnO is not the reason for the *E. coli* disinfection [24]. Some workers have also detected the generation of H_2O_2 by ZnO in absence of light [31] and have suggested the same as a main factor for the bacterial activity [27,31]. But the observed extent of inactivation of *E. coli* population in the present study (vide supra) makes the proposition unviable. As the antibacterial activities of some synthesized ZnO nanorods do not correlate with their photoluminescence features corresponding to surface defects (green emission) it has been concluded that the surface defects do not play any significant role in the antibacterial activity of ZnO [31]. The SEM and TEM images presented in a few reports show the binding of ZnO nanoparticles to the surface of *E. coli* bacteria [24,27,31]. There are several possible attachment mechanisms of the oxide to the bacterial surface: electrostatic forces, van der Waals forces and receptor-ligand interactions [24]. The zeta potential of ZnO suspended with *E. coli* at pH ~ 7 is approximately +24 mV [27]. The overall *E. coli* surface is negatively charged at neutral pH due to the polysaccharides of lipopolysaccharide, which predominate over the amide [27], and its potential is -7.2 mV at pH 6.5 [24]. Hence the interaction of ZnO with *E. coli* is favored by the electrostatic forces. The receptor-ligand interactions may dominate in the ZnO bound *E. coli* bacteria; carboxyl, amide, phosphate, hydroxyl groups and carbohydrate-related moieties in the bacterial cell wall may provide sites for the molecular-scale interactions with the oxide [24]. It has been reported that ZnO causes membrane damage, which leads to leakage of cell contents and cell death [31]. Further, only a few *E. coli* cells show internalization of ZnO nanoparticles while a large number of them do not exhibit such thing revealing that internalization is not a general occurrence [31]. The TEM displays also shrinkage of cytoplasmic material inside the cell wall of some of the *E. coli* cells [31]. The interaction of ZnO nanoparticles with the bacterial cell walls and possible permeation of ZnO into the bacterial cells are still not clearly understood [24]. It has been proposed that the induction of intracellular oxidative stress seems to be a key event of the toxicity mechanisms of many nanomaterials [25]. Once inside the cell, nanomaterials may induce intracellular oxidative stress by disturbing the balance between oxidant and anti-oxidant processes. On one hand, the oxidative stress induced by exposure to nanomaterials may stimulate an increase of the cytosolic calcium concentration or may cause the translocation of transcription factors to the nucleus, which regulate pro-inflammatory genes. Alternatively, exceeding oxidative stress may also modify proteins, lipids and nucleic acids, which further stimulates the anti-oxidant defense system or even leads to cell death.

4. Conclusions

ZnO wurtzite and TiO_2 anatase effectively catalyze degradation of 1-naphthol under UV light; the surfaces of CeO_2, CdO, WO_3, Co_3O_4, Sb_2O_3, ZrO_2, La_2O_3, Y_2O_3, Pr_6O_{11}, Sm_2O_3 and Al_2O_3 are less active to photodegrade 1-naphthol. The degradation essentially requires dissolved oxygen. ZnO, besides effectively photocatalytically degrading 1-naphthol, also acts as a bactericide; it inactivates *E.coli* even in absence of direct light. At a loading of 0.8 g L^{-1} it kills about 44% of 2.5×10^{12} CFU mL^{-1} *E. coli* in ½ h without any illumination.

Acknowledgements

The authors thank the Council of Scientific and Industrial Research (CSIR), New Delhi, for the financial support through research grant no. 01(2031)/06/EMR-II. Further, PG. is grateful to CSIR for JRF. The authors also thank Dr. J. Jayabharathi, Annamalai University for the DSR facility.

References

[1] J.D. Meeker, L. Ryan, D.B. Barr, R. Hauser, Exposure to nonpersistent insecticides and male reproductive hormones, Epidemiology 17 (2006) 61–68.
[2] S. Qourzal, N. Barka, M. Tamimi, A. Assabbane, A. Nounah, A. Ihlal, Y. Ait-Ichou, Sol-gel synthesis of TiO_2-SiO_2 photocatalyst for β-naphthol photodegradation, Mater. Sci. Eng. C 29 (2009) 1616–1620.
[3] S. Qourzal, N. Barka, M. Tamimi, A. Assabbane, Y. Ait-Ichou, Photodegradation of 2-naphthol in water by artificial light illumination using TiO_2 photocatalyst: identification of intermediates and the reaction pathway, Appl. Catal. A 334 (2008) 386–393.
[4] S. Qourzal, M. Tamimi, A. Assabbane, Y. Ait-Ichou, Influence de certains ions inorganiques, de l' ethanol et du peroxyde d'hydrogene sur la photominéralisation du β-naphtol en presence de TiO_2, C.R. Chimie 10 (2007) 1187–1194.
[5] T. Kawahara, K.-i. Yamada, H. Tada, Visible light photocatalytic decomposition of 2-naphthol by anodic-biased α-Fe_2O_3 film, J. Colloid Interface Sci. 294 (2006) 504–507.
[6] S. Qourzal, M. Tamimi, A. Assabbane, Y. Ait-Ichou, Photocatalytic degradation and adsorption of 2-naphthol on suspended TiO_2 surface in a dynamic reactor, J. Colloid Interface Sci. 286 (2005) 621–626.
[7] S. Qourzal, A. Assabbane, Y. Ait-Ichou, Synthesis of TiO_2 via hydrolysis of titanium tetraisopropoxide and its photocatalytic activity on a suspended mixture with activated carbon in the degradation of 2-naphthol, J. Photochem. Photobiol. A 163 (2004) 317–321.
[8] A. Renglin, A. Olsson, C.A. Wachtmeister, A. Onfelt, Mitotic disturbance by carbaryl and the metabolite 1-naphthol may involve kinase-mediated phosphorylation of 1-naphthol to the protein phosphatase inhibitor 1-naphthylphosphate, Mutagenesis 13 (1998) 345–352.
[9] T.L. Thompson, J.T. Yates Jr., Surface science studies of the photoactivation of TiO_2–new photochemical processes, Chem. Rev. 106 (2006) 4428–4453.
[10] Y. Tamaki, A. Furube, M. Murai, K. Hara, R. Kotoh, M. Tachiya, Direct observation of reactive trapped holes in TiO_2 undergoing photocatalytic oxidation of adsorbed alcohols: Evaluation of the reaction rates and yields, J. Am. Chem. Soc. 128 (2006) 416–417.
[11] Z. Guo, R. Ma, G. Li, Degradation of phenol by nanomaterial TiO_2 in wastewater, Chem. Eng. J. 119 (2006) 55–59.
[12] R. Enriquez, A.G. Agrios, P. Pichat, Probing multiple effects of TiO_2 sintering temperature on photocatalytic activity in water by use of a series of organic pollutant molecules, Catal. Today 120 (2007) 196–212.
[13] A. Sobczynski, L. Duczmal, W. Zmudzinski, Phenol destruction by photocatalysis on TiO_2: an attempt to solve the reaction mechanism, J. Mol. Catal. A 213 (2004) 225–230.
[14] M.H. Priya, G. Madras, Kinetics of photocatalytic degradation of phenols with multiple substituent groups, J. Photochem. Photobiol. A 179 (2006) 256–262.
[15] R. Osgood, Photoreaction dynamics of molecular adsorbates on semiconductor and oxide surfaces, Chem. Rev. 106 (2006) 4379–4401.
[16] J. Zhao, B. Li, K. Onda, M. Feng, H. Petek, Solvated electron on metal oxide surfaces, Chem. Rev. 106 (2006) 4402–4427.
[17] Y. Shiraishi, N. Saito, T. Hirai, Adsorption-driven photocatalytic activity of mesoporous titanium dioxide, J. Am. Chem. Soc. 127 (2005) 12820–12822.
[18] J. Peller, O. Wiest, P.V. Kamat, Hydroxyl radical's role in the remediation of a common herbicide, 2,4-dichlorophenoxyacetic acid (2,4-D), J. Phys. Chem. A 108 (2004) 10925–10933.
[19] Y. Du, J. Rabani, The measure of TiO_2 photocatalytic efficiency and the comparison of different photocatalytic titania, J. Phys. Chem. B 107 (2003) 11970–11978.
[20] L. Sun, J.R. Bolton, Determination of the quantum yield for the photochemical generation of hydroxyl radicals in TiO_2 suspensions, J. Phys. Chem. 100 (1996) 4127–4134.
[21] A. Fujishima, T.N. Rao, D.A. Tryk, Titanium dioxide photocatalysis, J. Photochem. Photobiol. C 1 (2000) 1–21.
[22] U.I. Gaya, A.H. Abdullah, Heterogeneous photocatalytic degradation of organic contaminants over titanium dioxide: a review of fundamentals, progress and problems, J. Photochem. Photobiol. C 9 (2008) 1–12.
[23] Y. Xu, M.A.A. Schoonen, The absolute energy position of conduction and valence bands of selected semiconducting minerals, Am. Mineral. 85 (2000) 543–556.
[24] W. Jiang, H. Mashayekhi, B. Xing, Bacterial toxicity comparison between nano- and micro-scaled oxide particles, Environ. Pollut. 157 (2009) 1619–1625.
[25] X. Hu, S. Cook, P. Wang, H.-m. Hwang, *In vitro* evaluation of cytotoxicity of engineered metal oxide nanoparticles, Sci. Total Environ. 407 (2009) 3070–3072.

[26] H.J. Kuhn, S.E. Braslavsky, R. Schmidt, Chemical actinometry (IUPAC technical report), Pure Appl. Chem. 76 (2004) 2105–2146.
[27] L. Zhang, Y. Ding, M. Povey, D. York, ZnO nanofluids–a potential antibacterial agent, Prog. Nat. Sci. 18 (2008) 939–944.
[28] T.R. Hinklin, R.M. Laine, Synthesis of metastable phases in the magnesium spinel-alumina system, Chem. Mater. 20 (2008) 553–558.
[29] C. Karunakaran, S. Senthilvelan, S. Karuthapandian, TiO_2-photocatalyzed oxidation of aniline, J. Photochem. Photobiol. A 172 (2005) 207–213.
[30] L. Vincze, T.J. Kemp, Light flux and light flux density dependence of the photomineralization rate of 2,4-dichlorophenol and chloroacetic acid in the presence of TiO_2, J. Photochem. Photobiol. A 87 (1995) 257–260.
[31] K.H. Tam, A.B. Djurisic, C.M.N. Chan, Y.Y. Xi, C.W. Tse, Y.H. Leung, W.K. Chan, F.C.C. Leung, D.W.T. Au, Antibacterial activity of ZnO nanorods prepared by a hydrothermal method, Thin Solid Films 516 (2008) 6167–6174.